File name: Supplementary Information
Description: Supplementary figures.

File name: Peer review file
Description:

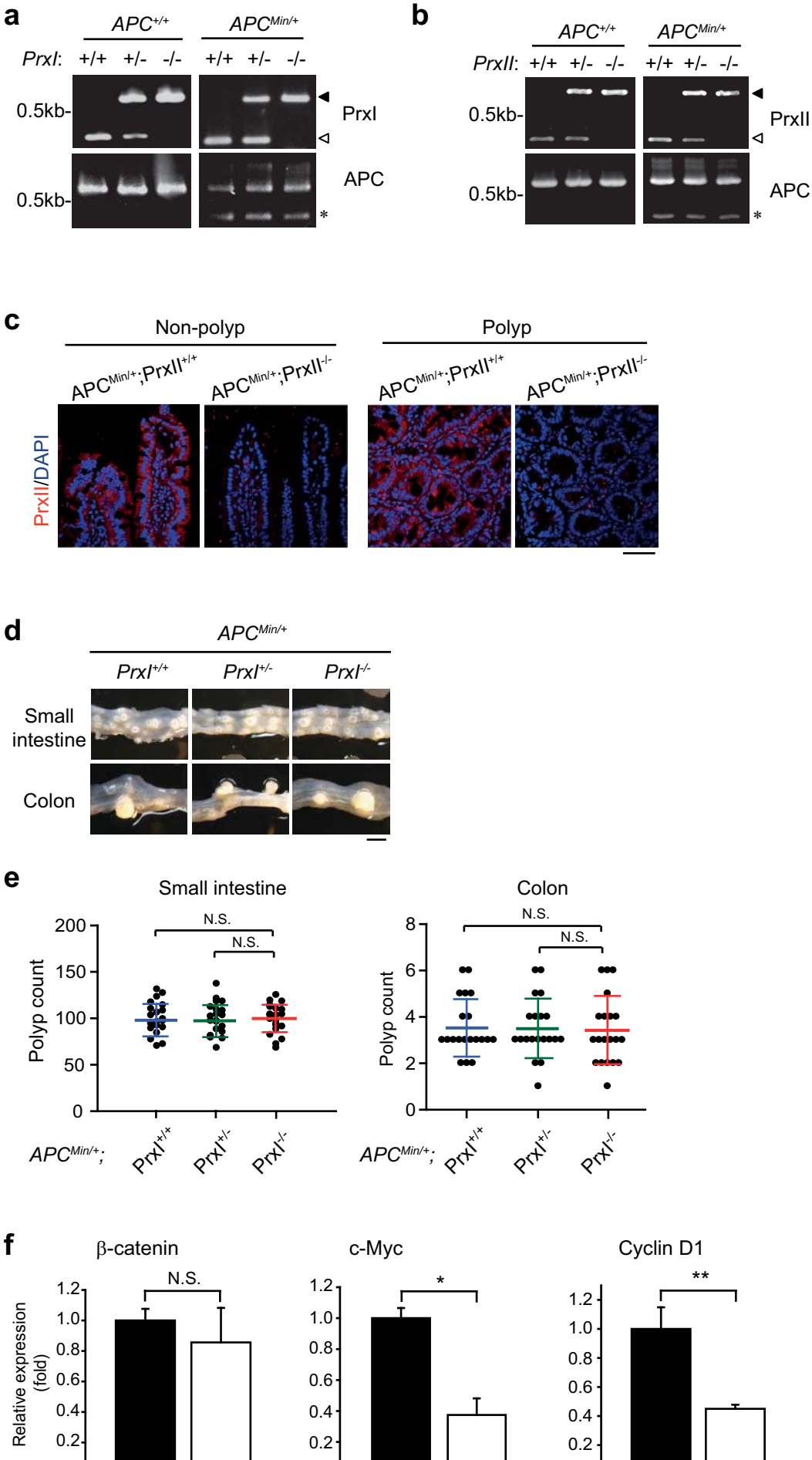
a
APC+/+
APCMin/+
PrxI: +/+ +/- -/-
+/+ +/- -/-
0.5kb-
PrxI
APC
b
PrxII
c
Non-polyp
Polyp
APCMin/+;PrxII+/+
APCMin/+;PrxII-/-
PrxII/DAPI
d
APCMin/+
PrxI+/+
PrxI+/-
PrxI-/-
Small intestine
Colon
e
Small intestine
Colon
Polyp count
N.S.
APCMin/+;
f
β-catenin
c-Myc
Cyclin D1
Axin1
Relative expression (fold)
PrxII+/+
PrxII-/-

Supplementary Fig. 1. Deletion of PrxI and PrxII in *APC*$^{Min/+}$ mice.

a and **b**. The double mutant mice were generated by mating *PrxI*$^{+/-}$ or *PrxII*$^{+/-}$ mice with *APC*$^{Min/+}$ mice. Mice were genotyped at 4 weeks by genomic PCR. The gene products for *PrxI/II*$^{+/+}$ and *PrxI/II*$^{-/-}$ mice are indicated by arrowheads (wild type, *closed arrowhead*; neo cassette, *filled arrowhead*). The gene product for truncated *APC* gene is indicated by an asterisk. The DNA size markers are labeled in kilobases (kb).

c. PrxII protein expression shown by immunofluorescence staining in non-polyp segments and polyps in the small intestine. Nuclei were stained with DAPI. Scale bar, 50 μm.

d. Representative photomicrographs of longitudinally-opened intestinal tissues from *APC*$^{Min/+}$*;PrxI*$^{+/+}$, *APC*$^{Min/+}$*;PrxI*$^{+/-}$, and *APC*$^{Min/+}$*;PrxI*$^{-/-}$ mice. Scale bar, 5 mm.

e. The macroscopic polyps (> 3 mm in diameter) were counted in whole-mount intestinal tissues from *APC*$^{Min/+}$;*PrxI*$^{+/+}$, *APC*$^{Min/+}$;*PrxI*$^{+/-}$, and *APC*$^{Min/+}$;*PrxI*$^{-/-}$ mice. Dot plots represent the average polyp numbers ± SD (n = 20 mice per group, P = 0.9144 (small intestine) and 0.7282 (colon) for *APC*$^{Min/+}$;*PrxI*$^{+/+}$ vs *APC*$^{Min/+}$;*PrxI*$^{-/-}$, P = 0.8592 (small intestine) and 0.8193 (colon) for *APC*$^{Min/+}$;*PrxI*$^{+/-}$ vs *APC*$^{Min/+}$;*PrxI*$^{-/-}$ with repeated measures ANOVA). N.S., not significant.

f. Expression of Axin1, β-catenin, and β-catenin target genes in polyps from *APC*$^{Min/+}$;*PrxII*$^{+/+}$ and *APC*$^{Min/+}$;*PrxII*$^{-/-}$ mice. Level of mRNA was measured by quantitative real-time PCR as described in *Methods*. Data in the graph are means ± SD of fold change in mRNA level versus that of *APC*$^{Min/+}$;*PrxII*$^{+/+}$ mice (n = 4 mice per group; $^{*}P < 0.01$; $^{**}P < 0.001$). N.S., not significant.

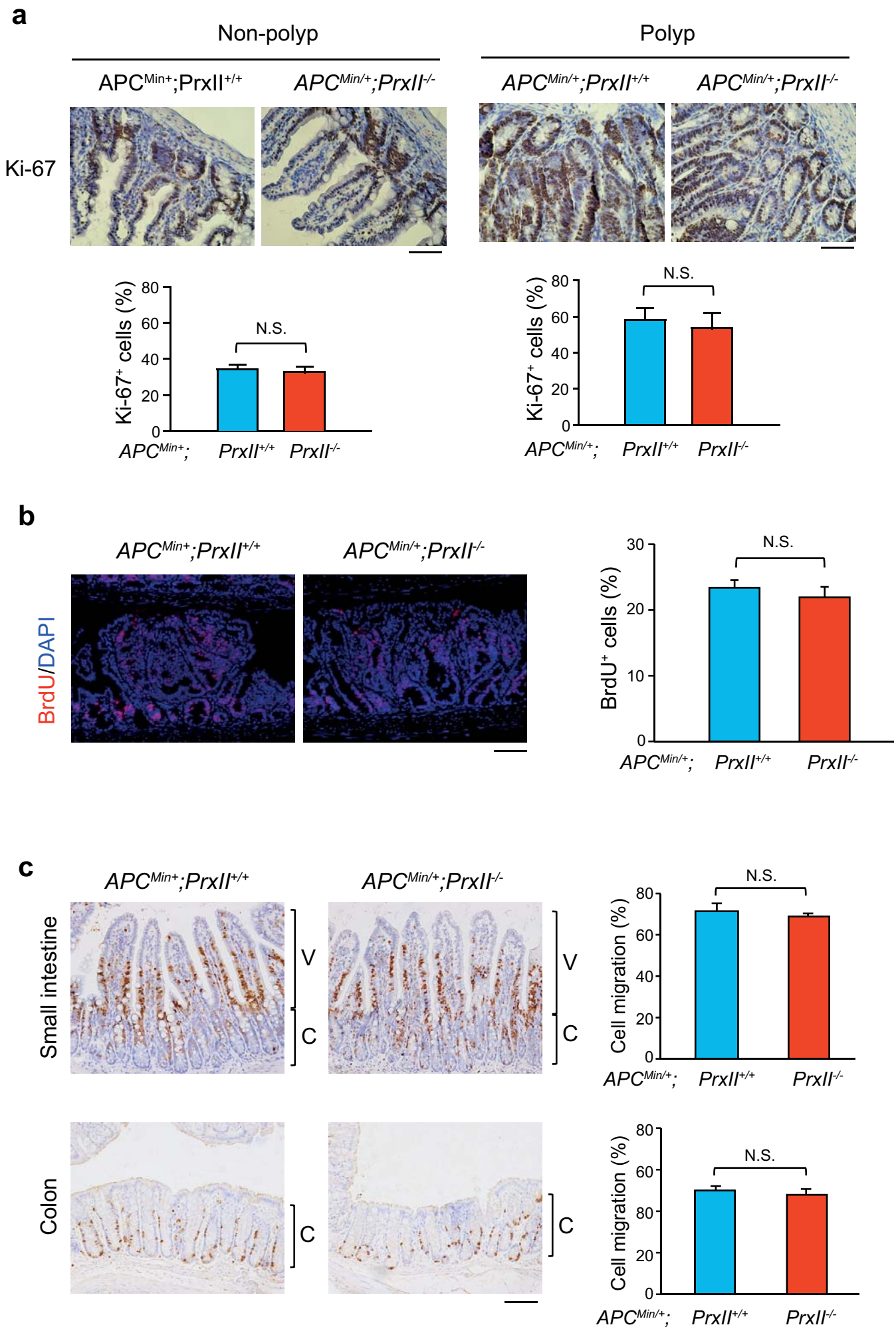
a
Non-polyp
Polyp
APCMin+;PrxII+/+
APCMin/+;PrxII-/-
APCMin/+;PrxII+/+
APCMin/+;PrxII-/-
Ki-67
Ki-67+ cells (%)
80
60
40
20
0
N.S.
APCMin+;
PrxII+/+
PrxII-/-
Ki-67+ cells (%)
80
60
40
20
0
N.S.
APCMin/+;
PrxII+/+
PrxII-/-
b
APCMin+;PrxII+/+
APCMin/+;PrxII-/-
BrdU/DAPI
BrdU+ cells (%)
30
20
10
0
N.S.
APCMin/+;
PrxII+/+
PrxII-/-
c
APCMin+;PrxII+/+
APCMin/+;PrxII-/-
Small intestine
V
C
V
C
Cell migration (%)
80
60
40
20
0
N.S.
APCMin/+;
PrxII+/+
PrxII-/-
Colon
C
C
Cell migration (%)
80
60
40
20
0
N.S.
APCMin/+;
PrxII+/+
PrxII-/-

Supplementary Fig. 2. Proliferation and migration of epithelial cells in the intestinal polyps and villi of *APC*$^{Min/+}$;*PrxII*$^{+/+}$ and *APC*$^{Min/+}$;*PrxII*$^{-/-}$ mice.

a. Immunohistochemistry images for Ki-67 in the non-polyp segments and the polyps of *APC*$^{Min/+}$;*PrxII*$^{+/+}$ and *APC*$^{Min/+}$;*PrxII*$^{-/-}$ mice. DAB staining in the images was quantified using HistoFAXS (TissuGnostics). Data in the graph are means ± SD of the intensity measured (n = 5 per group, P = 0.3477 (non-polyp) and 0.3559 (polyp)). Scale bar, 50 μm.

b. Number of proliferating cells in the polyps in the small intestine. 5-bromo-2'-deoxyuridine (BrdU) incorporation was performed for 2 hr after intraperitoneal injection (0.1 ml injection of 10 mM BrdU in PBS per 10g body weight). Paraffin tissue sections were immunostained with anti-BrdU antibody. Cell numbers were counted using the Image J program. Data in the graph are means ± SEM of the number of BrdU-positive cells per polyp (n = 4 mice for *PrxII*$^{+/+}$, n = 3 mice for *PrxII*$^{-/-}$, P = 0.4816 with two-tailed t-test). Scale bar, 50 μm.

c. Migration of epithelial cells in the villi of small intestine and colon. BrdU incorporation was performed for 30 hr after intraperitoneal injection. Paraffin tissue sections were immunostained with anti-BrdU antibody. Cell migration was determined by measuring the length of the most migrating cell from bottom of crypt using NIS-Elements BR3.2 imaging software (Nikon). Data in the graph are means ± SEM of the percent of the length of most migrating cell per total length of villus (V) plus crypt (C) or crypt (n = 3 mice for *PrxII*$^{+/+}$, n = 5 mice for *PrxII*$^{-/-}$, P = 0.6159 (small intestine) and P = 0.1851 (colon) with two-tailed t-test). A representative image is shown. N.S., not significant. Scale bar, 50 μm.

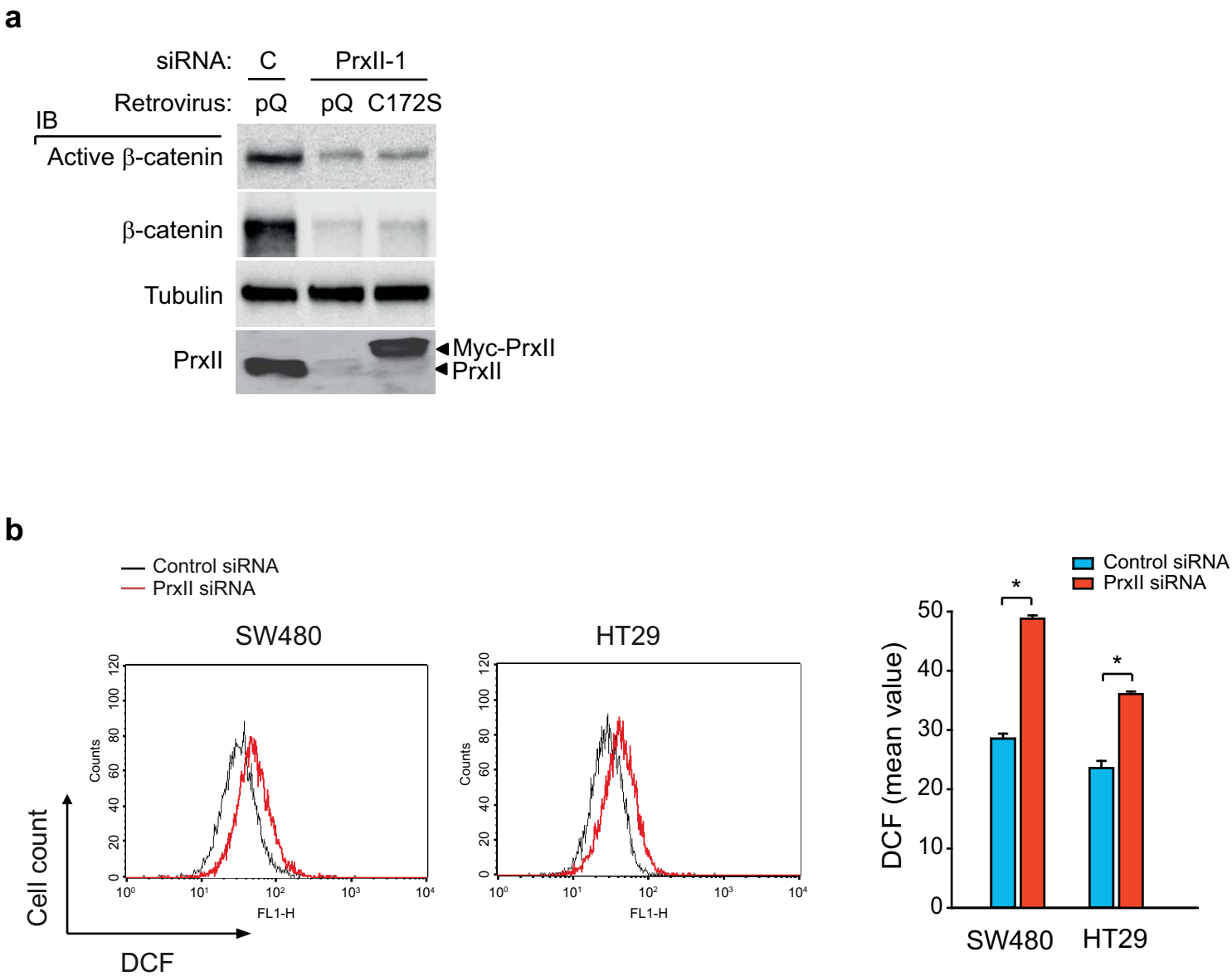

Supplementary Fig. 3. APC-dependent cellular H_2O_2 levels in CRC cells

a. HT29 cells were transfected with control or PrxII-1 siRNa for 24 hr and then infected with retroviruses expressing siRNA-resistant PrxII-C172S mutant with a Myc tag for additional 24 hr. Empty retrovirus (pQ) was used for control. The cell lysate were subjected to Western blotting for indicated proteins.

b. Intracellular H_2O_2 level was increased by PrxII depletion in SW480 and HT29 cells. CRC cells were transfected with control and PrxII-siRNA for 24 hr. Next day, cells were rinsed with a phenol-red-free basal medium and incubated with 5 μM 5,6-chloromethyl-2',7'-dichlorohydrofluorescein diacetate at 37 °C for 30 min. The cells were trypsinized and analyzed with a flow cytometry. Data in the graph are means ± SD of dichlorofluorescein (DCF) fluorescence values from three independent experiments ($^{*}P < 0.001$)

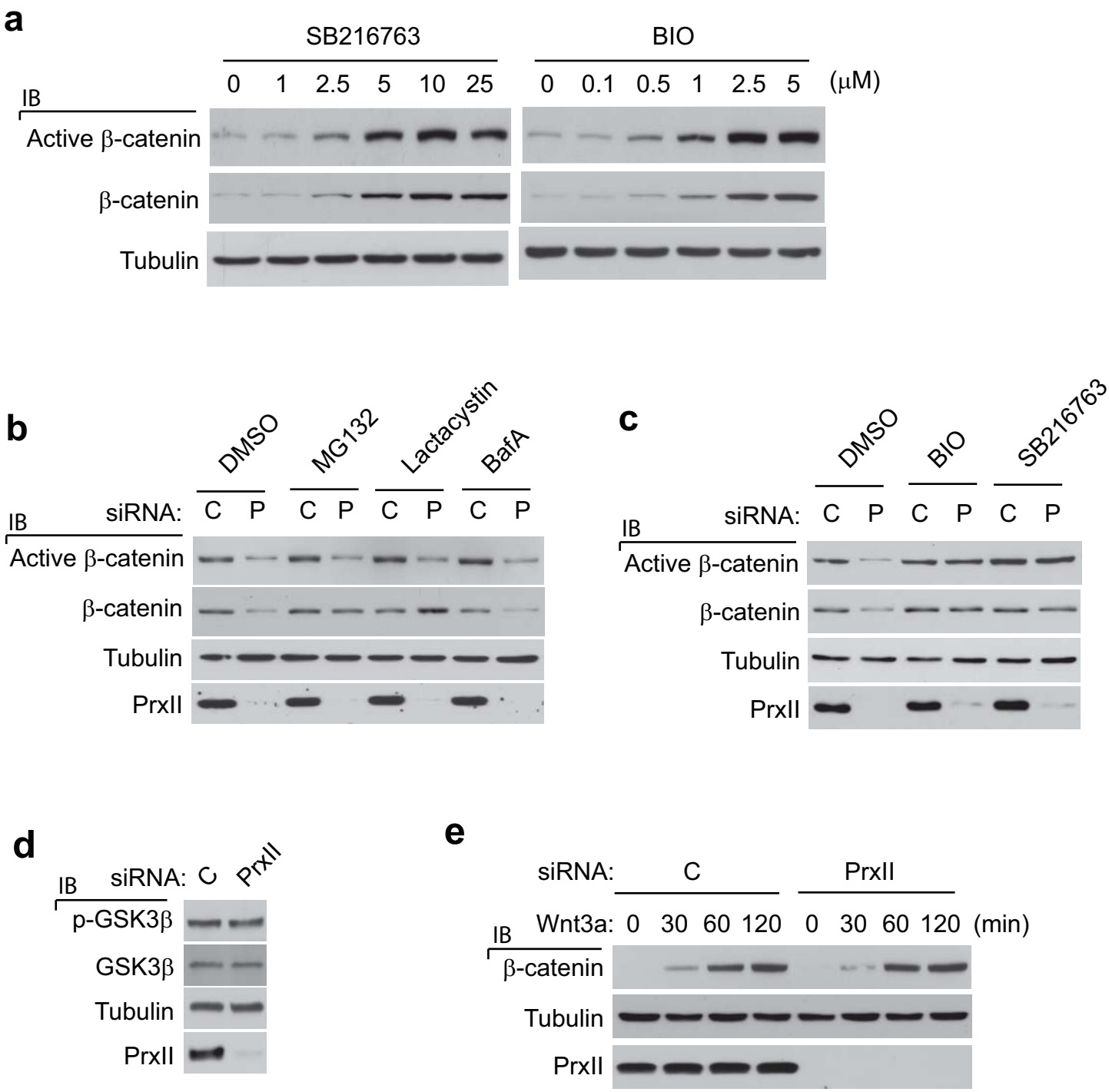
a
SB216763
BIO
0 1 2.5 5 10 25
0 0.1 0.5 1 2.5 5 (μM)
IB
Active β-catenin
β-catenin
Tubulin
b
DMSO
MG132
Lactacystin
BafA
siRNA: C P C P C P C P
IB
Active β-catenin
β-catenin
Tubulin
PrxII
c
DMSO
BIO
SB216763
siRNA: C P C P C P
IB
Active β-catenin
β-catenin
Tubulin
PrxII
d
siRNA: C PrxII
IB
p-GSK3β
GSK3β
Tubulin
PrxII
e
siRNA: C PrxII
Wnt3a: 0 30 60 120 0 30 60 120 (min)
IB
β-catenin
Tubulin
PrxII

Supplementary Fig. 4. Effect of proteasomal and GSK3β inhibition on PrxII-dependent β-catenin degradation in APC-mutant CRC cells.

a. Titration of GSK3β inhibitors (SB216763 and BIO) for β-catenin stabilization. HEK293 cells were treated with increasing concentrations of the indicated compounds and subjected to immunoblot (IB) analysis for total and active β-catenins. The optimal concentrations for maximum inhibition were determined to be 10 μM and 2.5 μM for SB216763 and BIO, respectively. Active β-catenin represents the transcriptionally active form unphosphorylated on Ser37/Thr41.

b and **c**. HT29 cells were transfected with control (C) and PrxII-1 siRNA for 24 hr and then treated with proteasome and GSK3β inhibitors (MG132, 25μM; lactacystin, 1μM; bafilomycin A1 (BafA), 100 nM; SB216763, 10 μM; BIO, 2.5 μM) for further 24 hr. The lysosomal inhibitor BafA did not restore the β-catenin level. Control vehicle was dimethyl sulfoxide (DMSO).

d. SW480 cells were transfected with control and PrxII-1 siRNA for 24 hr and immunoblotted for Y216 phosphorylation, an indicator of GSK3β activation.

e. HEK293 cells were transfected with control and PrxII-1 siRNA and then treated with Wnt3a (100 ng/ml) for the indicated times. The cytosolic fraction was isolated by ultracentrifugation and subjected to immunoblot analysis. A representative blot from three independent experiments is shown.

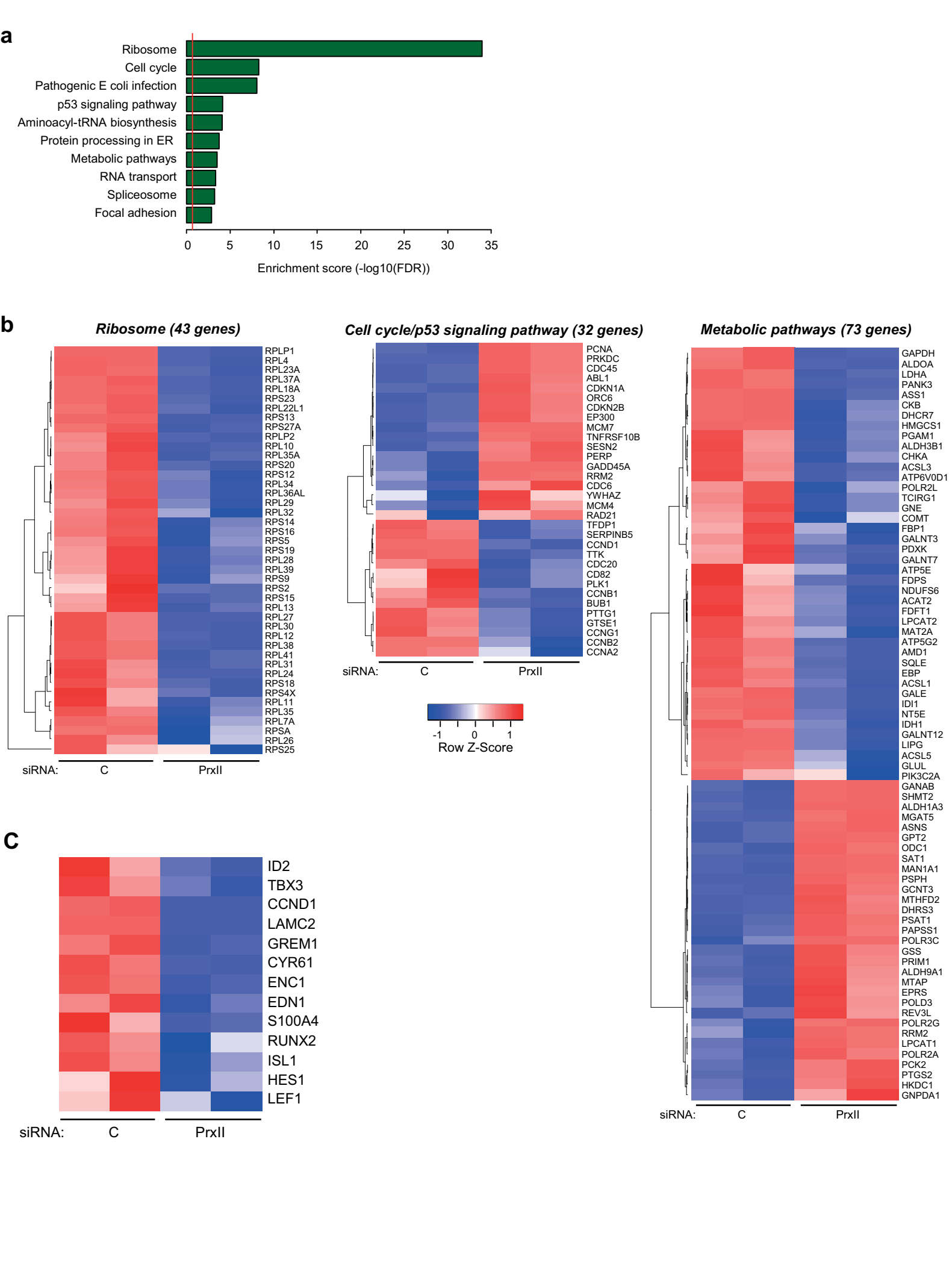
a
Ribosome
Cell cycle
Pathogenic E coli infection
p53 signaling pathway
Aminoacyl-tRNA biosynthesis
Protein processing in ER
Metabolic pathways
RNA transport
Spliceosome
Focal adhesion
0
5
10
15
20
25
30
35
Enrichment score (-log10(FDR))
b
Ribosome (43 genes)
RPLP1
RPL4
RPL23A
RPL37A
RPL18A
RPS23
RPL22L1
RPS13
RPS27A
RPLP2
RPL10
RPL35A
RPS20
RPS12
RPL34
RPL36AL
RPL29
RPL32
RPS14
RPS16
RPS5
RPS19
RPL28
RPL39
RPS9
RPS2
RPS15
RPL13
RPL27
RPL30
RPL12
RPL38
RPL41
RPL31
RPL24
RPS18
RPS4X
RPL11
RPL35
RPL7A
RPSA
RPL26
RPS25
siRNA:
C
PrxII
Cell cycle/p53 signaling pathway (32 genes)
PCNA
PRKDC
CDC45
ABL1
CDKN1A
ORC6
CDKN2B
EP300
MCM7
TNFRSF10B
SESN2
PERP
GADD45A
RRM2
CDC6
YWHAZ
MCM4
RAD21
TFDP1
SERPINB5
CCND1
TTK
CDC20
CD82
PLK1
CCNB1
BUB1
PTTG1
GTSE1
CCNG1
CCNB2
CCNA2
siRNA:
C
PrxII
-1
0
1
Row Z-Score
Metabolic pathways (73 genes)
GAPDH
ALDOA
LDHA
PANK3
ASS1
CKB
DHCR7
HMGCS1
PGAM1
ALDH3B1
CHKA
ACSL3
ATP6V0D1
POLR2L
TCIRG1
GNE
COMT
FBP1
GALNT3
PDXK
GALNT7
ATP5E
FDPS
NDUFS6
ACAT2
FDFT1
LPCAT2
MAT2A
ATP5G2
AMD1
SQLE
EBP
ACSL1
GALE
IDI1
NT5E
IDH1
GALNT12
LIPG
ACSL5
GLUL
PIK3C2A
GANAB
SHMT2
ALDH1A3
MGAT5
ASNS
GPT2
ODC1
SAT1
MAN1A1
PSPH
GCNT3
MTHFD2
DHRS3
PSAT1
PAPSS1
POLR3C
GSS
PRIM1
ALDH9A1
MTAP
EPRS
POLD3
REV3L
POLR2G
RRM2
LPCAT1
POLR2A
PCK2
PTGS2
HKDC1
GNPDA1
siRNA:
C
PrxII
c
ID2
TBX3
CCND1
LAMC2
GREM1
CYR61
ENC1
EDN1
S100A4
RUNX2
ISL1
HES1
LEF1
siRNA:
C
PrxII

Supplementary Fig. 5. Analysis of differentially expressed genes in HT29 cells after PrxII depletion.

RNA-Seq was performed as described in *Methods*. The 789 differentially-expressed genes (DEG) were identified with false discovery rate (FDR) cut-off 0.05 and then analyzed for KEGG pathway.

a. Bar plot showing top 10 KEGG pathways with significant FDR values.

b. Heat map depicting the list of DEGs belonging to representative KEGG pathways. Duplicate experimental data sets are shown in parallel.

c. Heat map depicting the significant downregulation of β-catenin/TCF-dependent gene expression by PrxII depletion in SW480 cells. Duplicate experiments are shown in parallel.

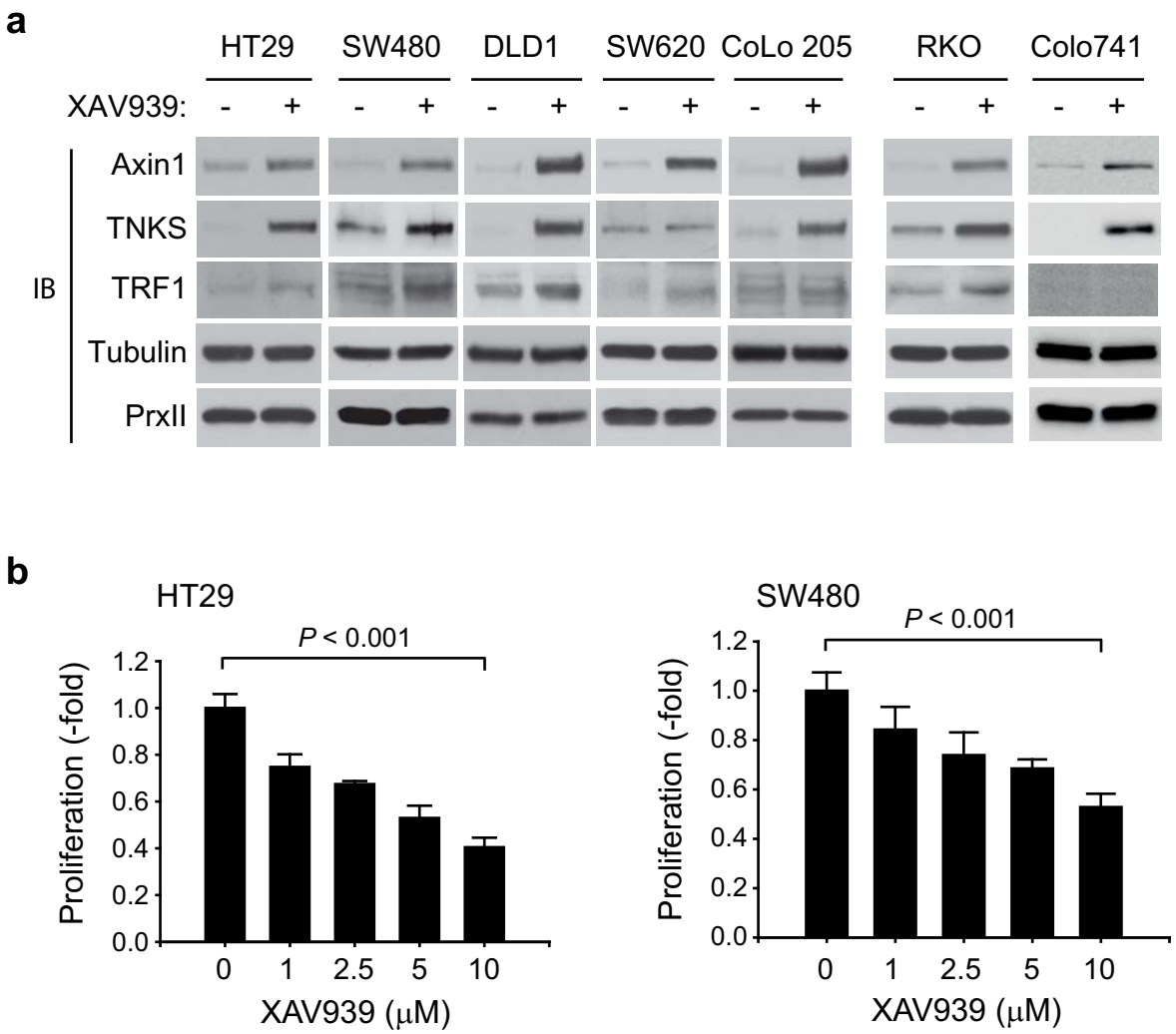

Supplementary Fig 6. Levels of TNKS and its substrate proteins in APC-mutant CRC cells treated with a TNKS inhibitor XAV939.

a. CRC cells were treated with DMSO vehicle control or TNKS inhibitor XAV939 (1μM) for 18 hr and then subjected to Western blot analysis for indicted proteins. HT29 and CoLo205 cells were exceptionally treated with 5 μM XAV939 for 18 hr. Immunoblot (IB) is a representative of two independent experiments with the same results.

b. HT29 and SW480 cells were treated with indicated concentrations of XAV939 for 36 hr. Cell number were measured with WST-1 reagent (Roche) according to manufacturer's protocol. Data in the graph show means ± SD of fold changes versus untreated sample (n = 3). P values are indicated.

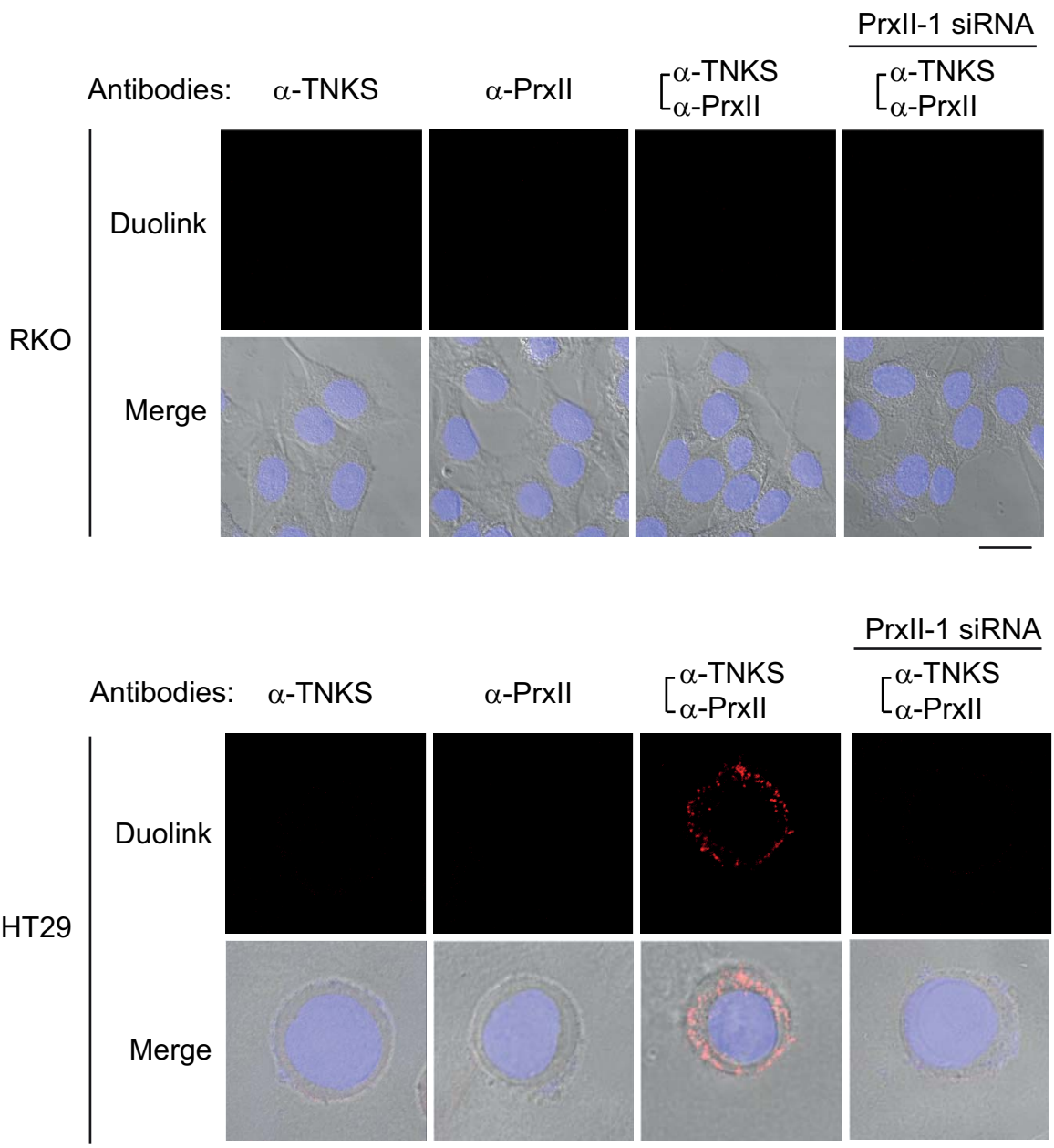

Supplementary Fig. 7. Proximal ligation assay shows direct interaction between TNKS and PrxII in the cytosol of APC-mutant CRC cells.

An *in situ* proximal ligation assay to detect binding between TNKS and PrxII proteins was performed in RKO and HT29 cells using DuoLink® *in situ* probes with the indicated antibodies. DuoLink Red fluorescence was detected only by the combination of anti-TNKS and anti-PrxII antibodies, not by single antibodies, which suggests a specific interaction between TNKS and PrxII. As a negative control, CRC cells were transfected with PrxII-1 siRNA. DIC and DAPI-stained images were merged with DuoLink fluorescence images (Merge). A representative image from three independent experiments is shown. Scale bar, 20 μm (RKO) and 10 μm (HT29).

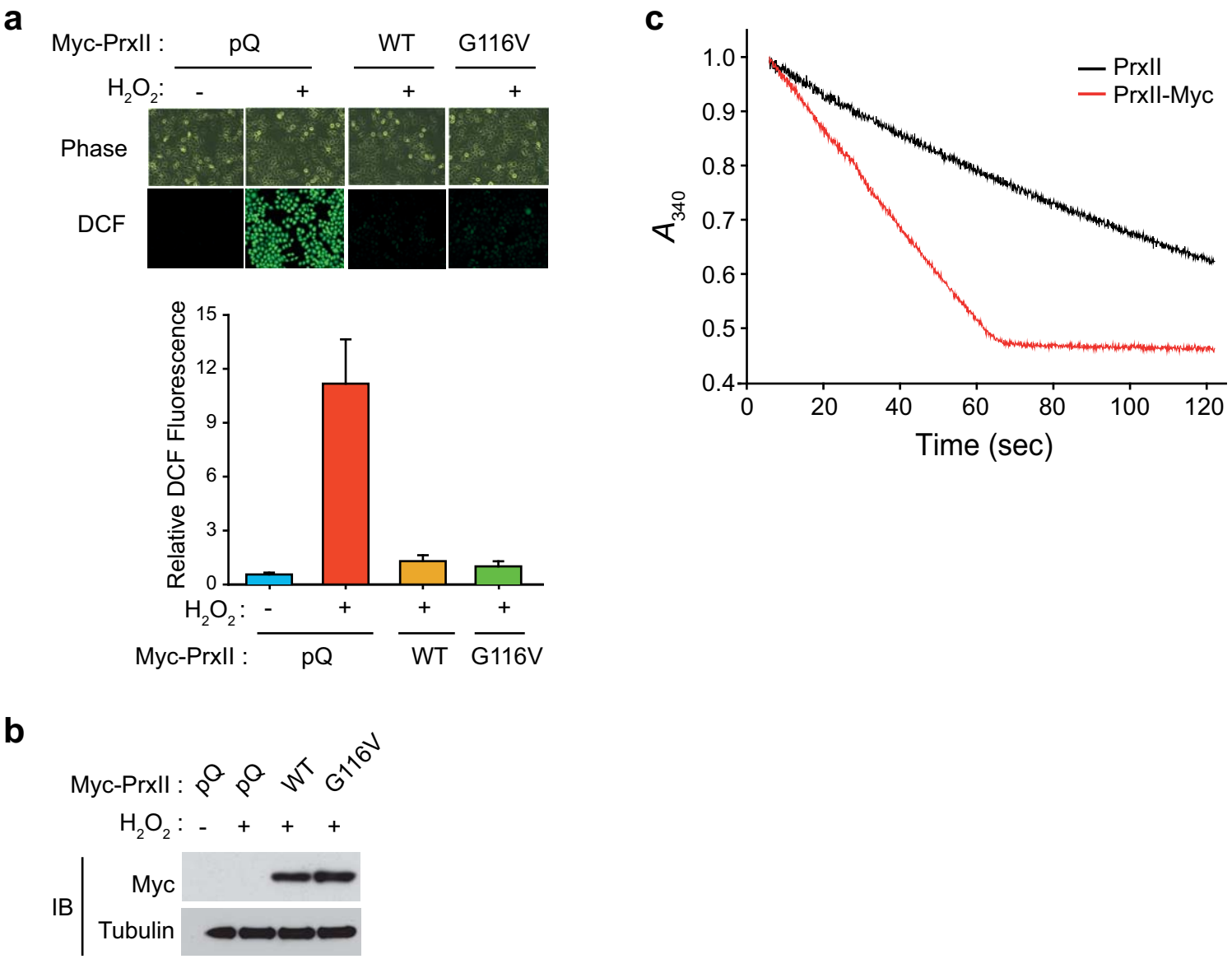

Supplementary Fig. 8. Peroxidase activity of the PrxII G116V mutant and PrxII with a Myc tag.

a. Cellular peroxidase activities were measured using an H_2O_2-sensitive fluorescence probe, 5,6-chloromethyl-2′,7′-dichlorodihydrofluorescein diacetate. HEK293 cells were infected with retroviruses expressing WT and G116V mutant of Myc-tagged PrxII for 24 hr. The cells were treated with 100μM H_2O_2 for 10 min, washed with a phenol-red-free basal medium, and incubated with 5 μM 5,6-chloromethyl-2′,7′-dichlorodihydrofluorescein diacetate at 37°C for 5 min. The dichlorofluorescein (DCF) fluorescence images were taken by a fluorescence microscope (Axiovert 200 Basic standard, Zeiss, Germany). The relative DCF fluorescence was calculated by averaging the fluorescence levels from 50 - 80 cells after subtracting the background fluorescence. Data in the graph are means ± SD of relative DCF fluorescence values from three independent experiments.

b. Immunoblotting (IB) was performed for checking the expression of indicated proteins. The empty retrovirus (pQ) was used for control.

c. Peroxidase activity assay using purified recombinant proteins of PrxII and PrxII with a Myc tag (PrxII-Myc) was performed in a reaction mixture containing 50mM HEPES (pH7.0), 4.3 μM human Trx, 0.165 μM rat liver TrxR, 200 μM NADPH, 100μM H_2O_2, and 3.4μM PrxII.

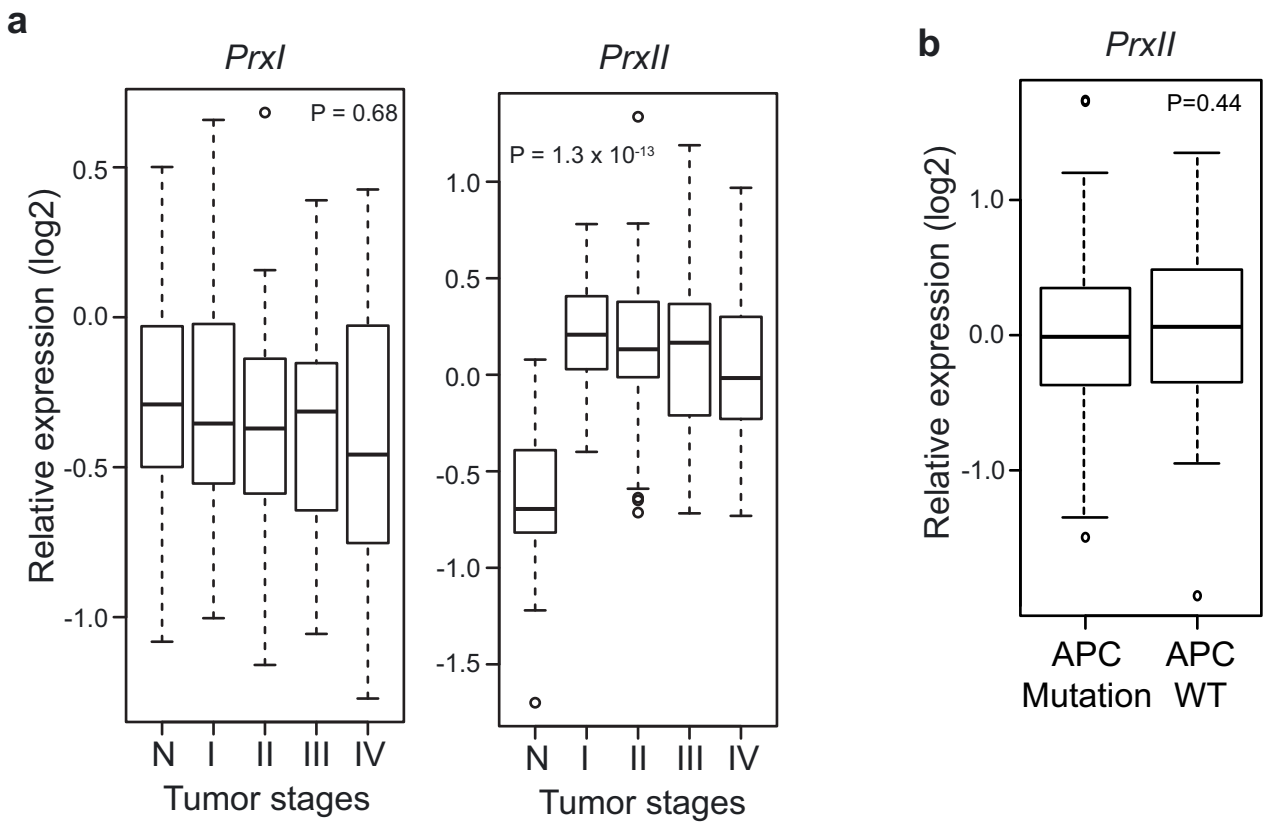

Supplementary Fig. 9. Increased expression of *PrxII* genes in patients with colorectal cancer.

a. Tumor stage-dependent expression of *PrxI* and *PrxII* genes, N, normal.

b. Expression levels of PrxII gene in colon cancer patients with APC WT (n = 45) and APC mutation (n = 104). The GA platform data (n = 149) from TCGA COAD database were used for analysis.

Box plot represents the average expression of PrxI and PrxII ± SD. The horizontal line indicates the median value.

Supplementary Fig 10 Uncropped images of all the western blot data

Figure 1e

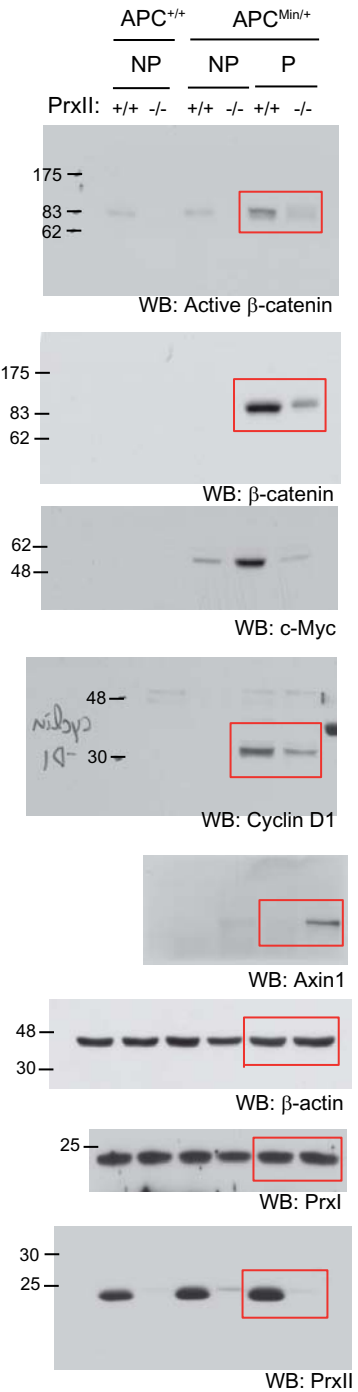

Figure 2a

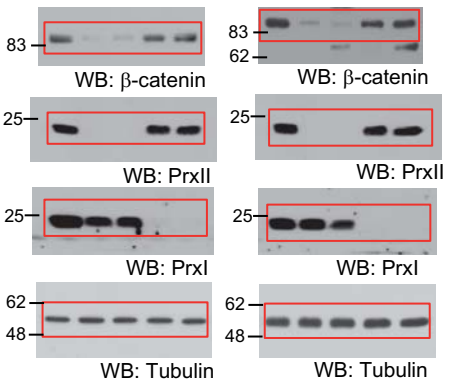

Figure 2b

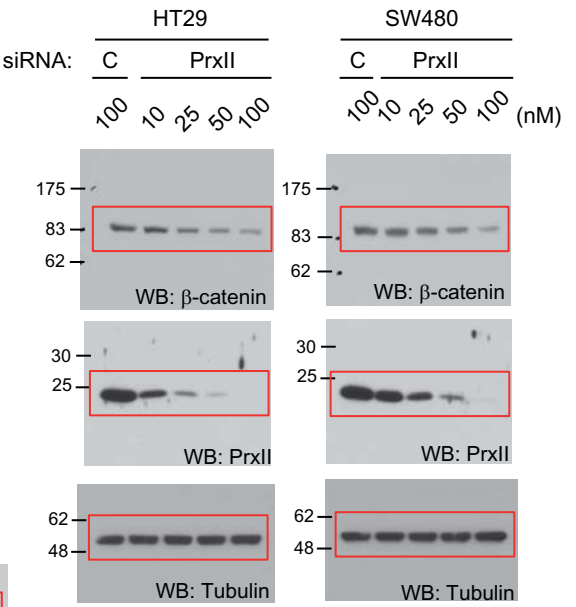

Figure 2c

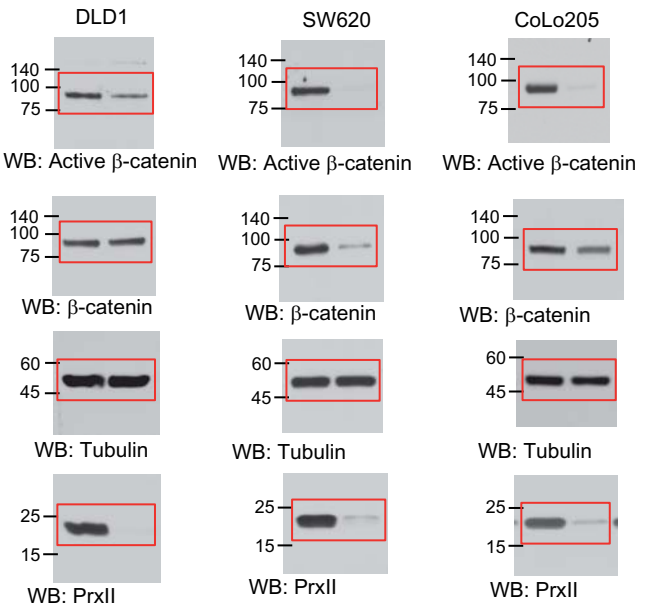

Figure 2d

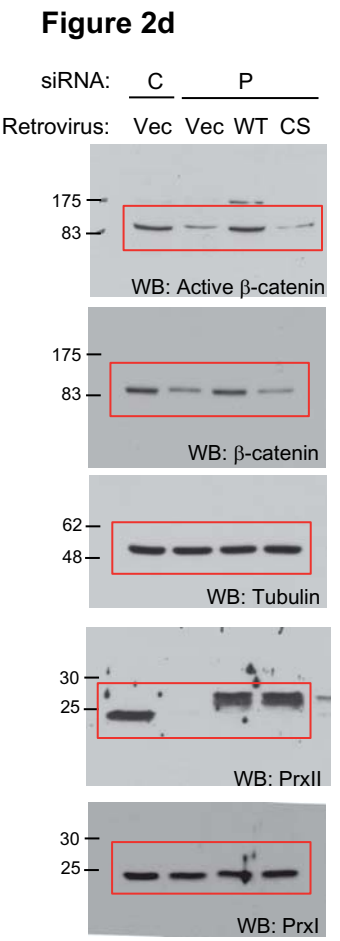

Figure 2e

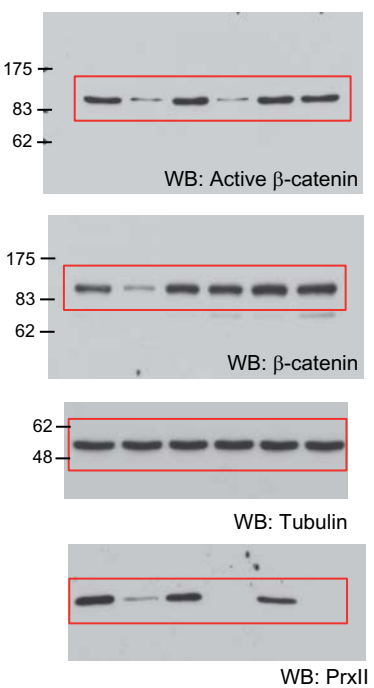

Supplementary Fig 10 Continued

Figure 3a

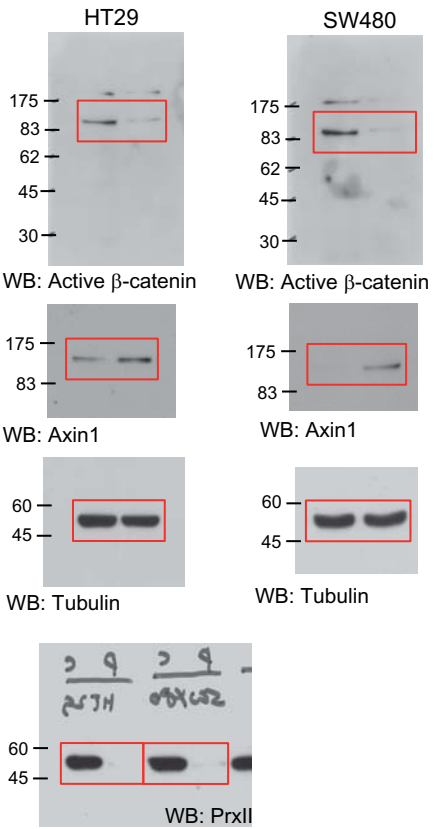

Figure 3b

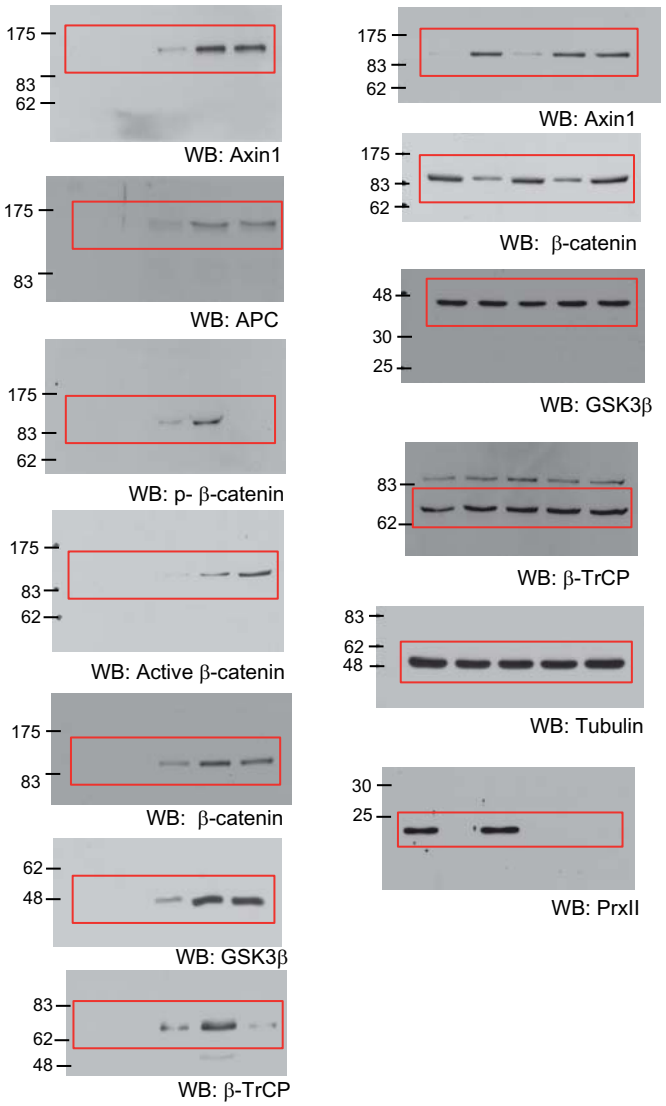

Figure 3c

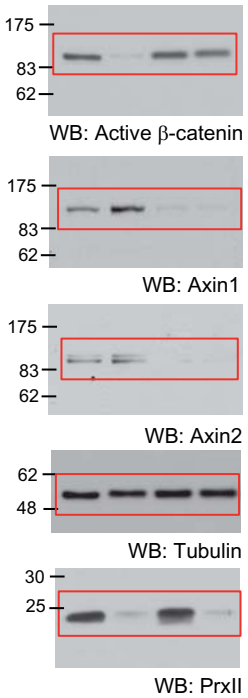

Figure 3d

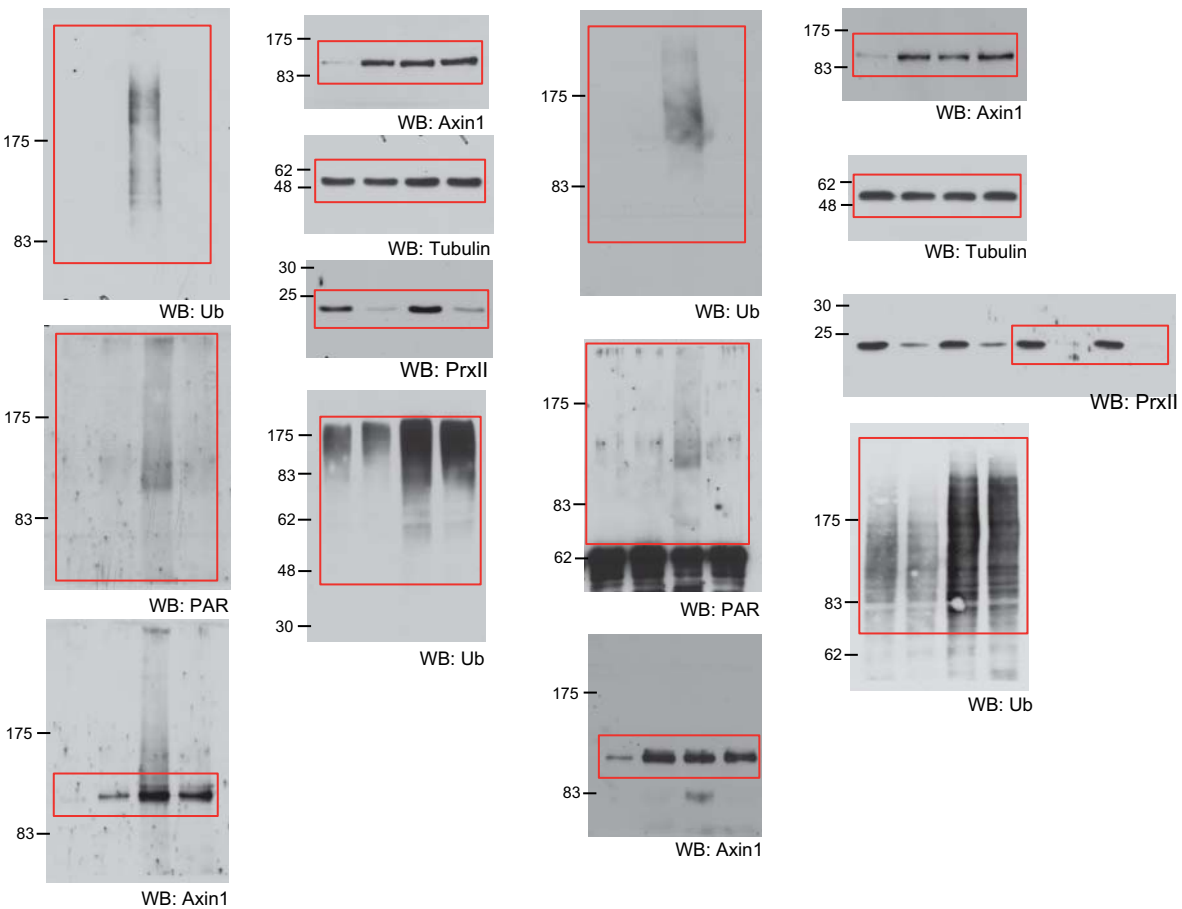

Supplementary Fig 10 Continued

Figure 4a/b

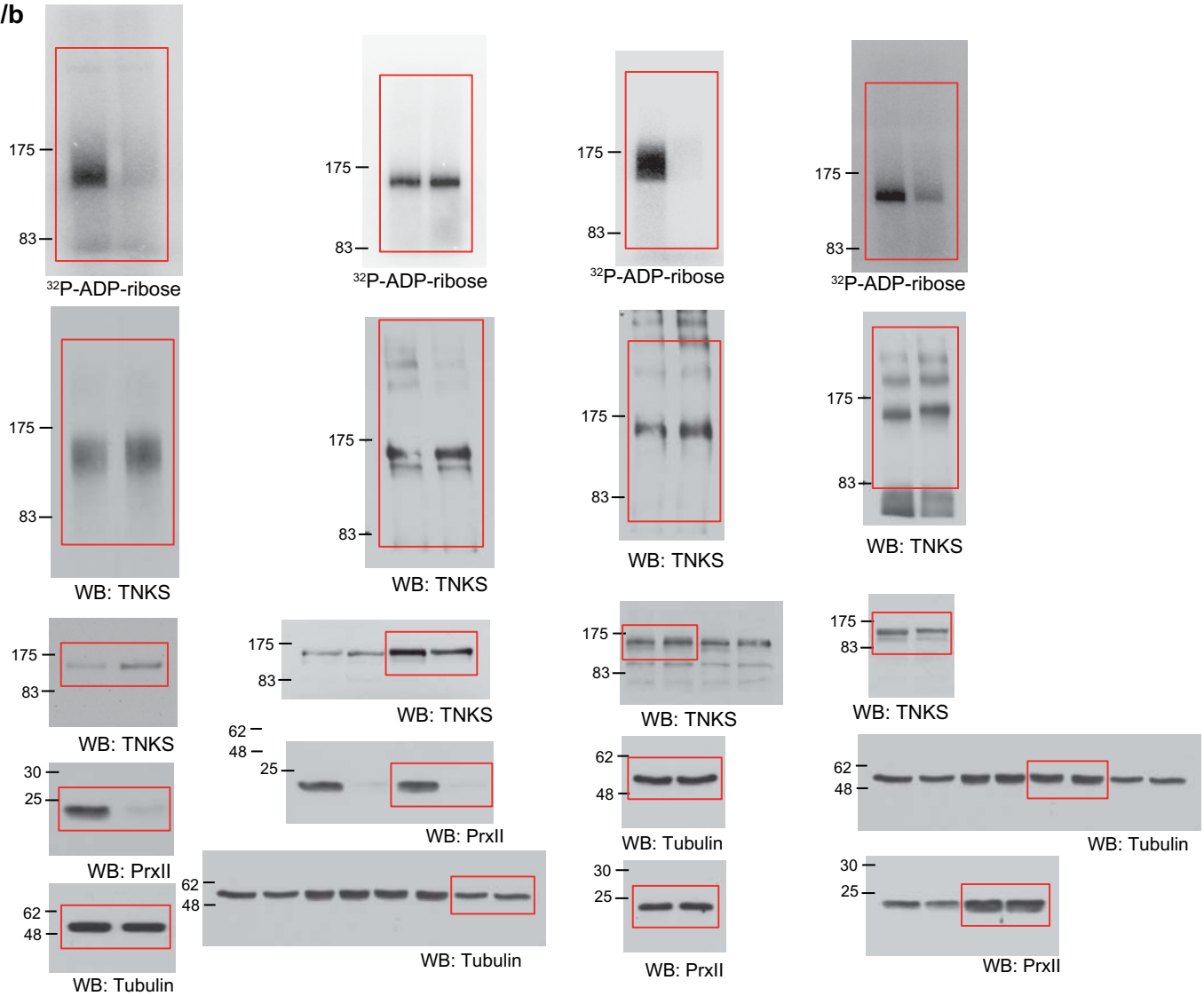

Figure 4C

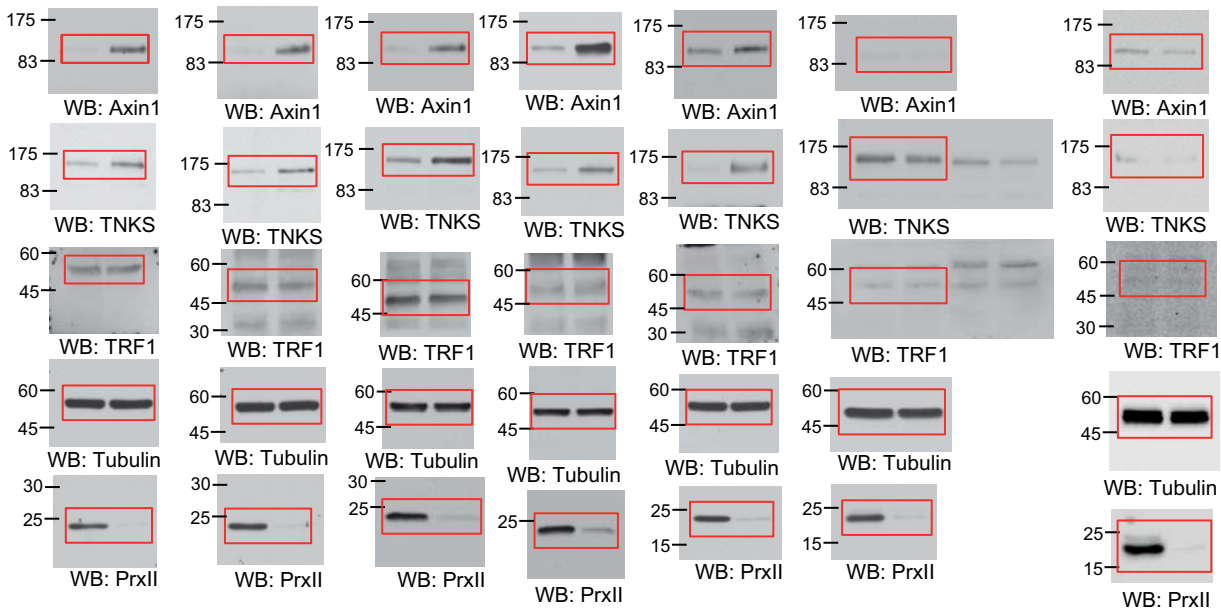

Figure 4d

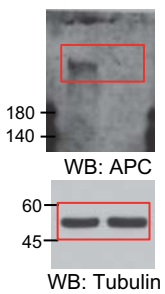

Supplementary Fig 10 Continued

Figure 4e

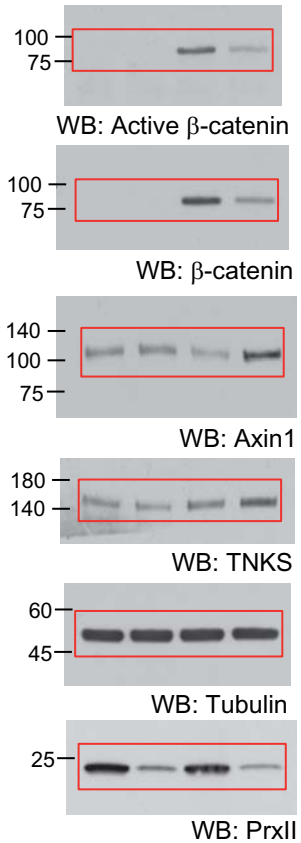

Figure 4f

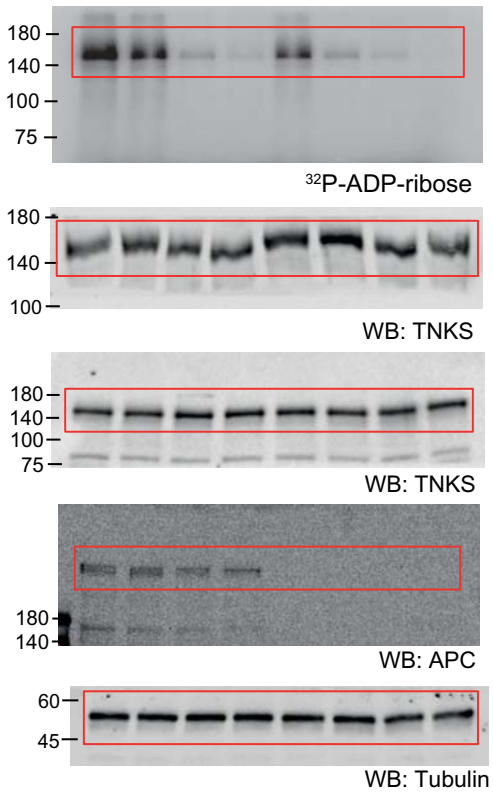

Figure 4g

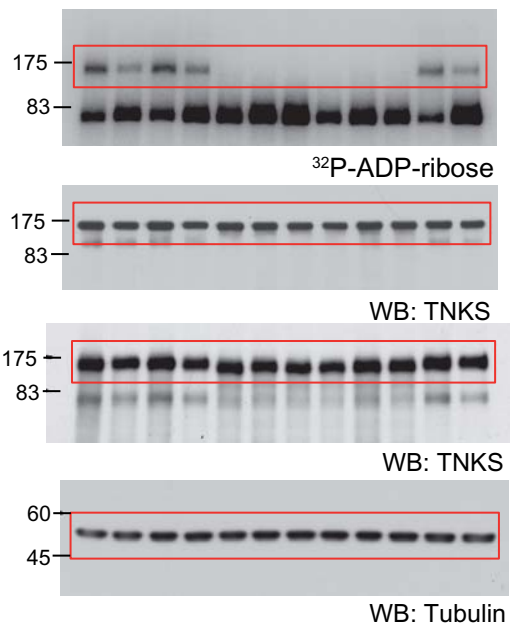

Figure 4h

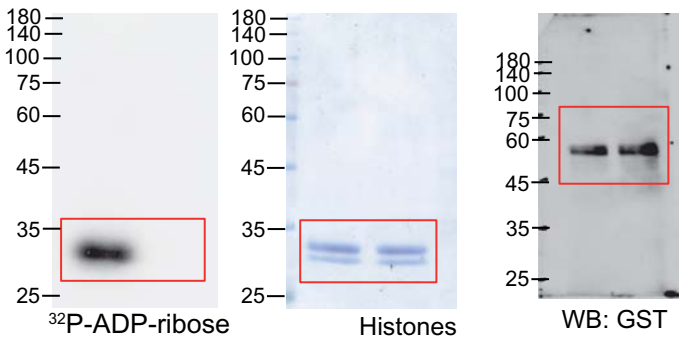

Supplementary Fig 10 Continued

Figure 5a

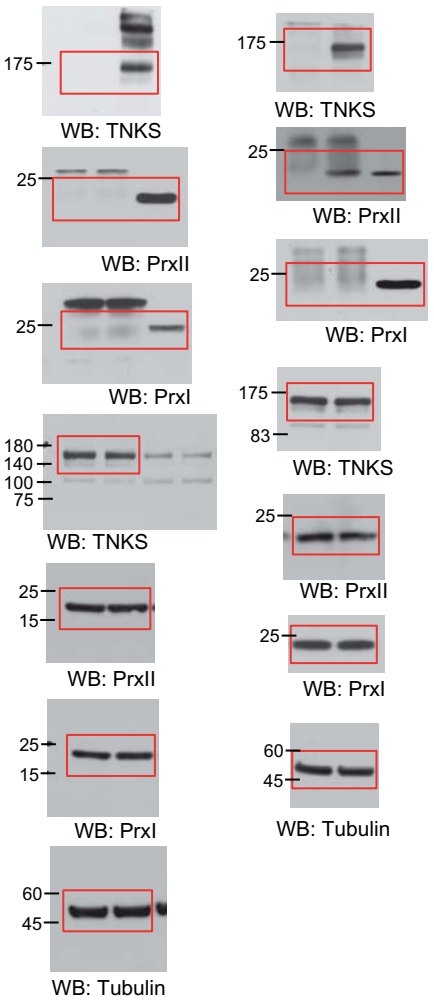

Figure 5b

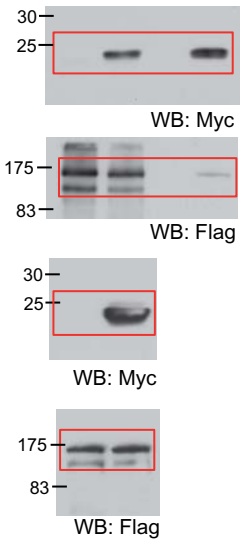

Figure 5d

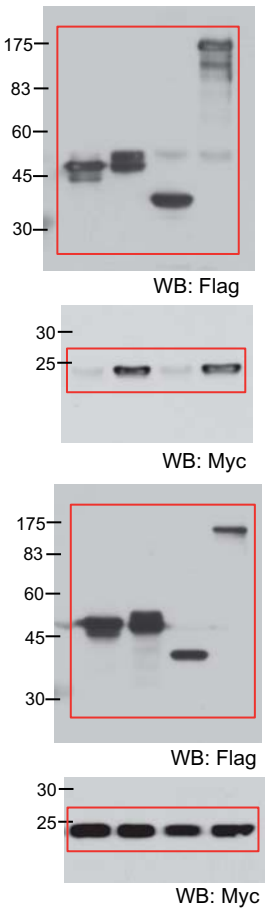

Figure 5e

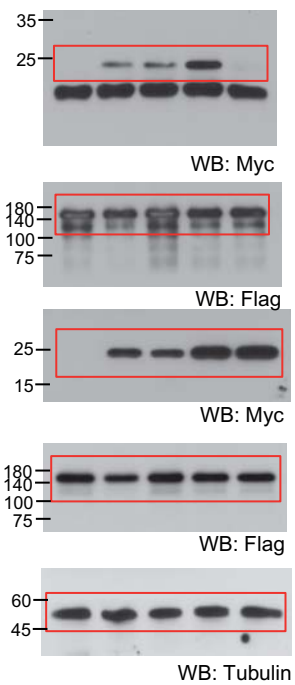

Figure 5f

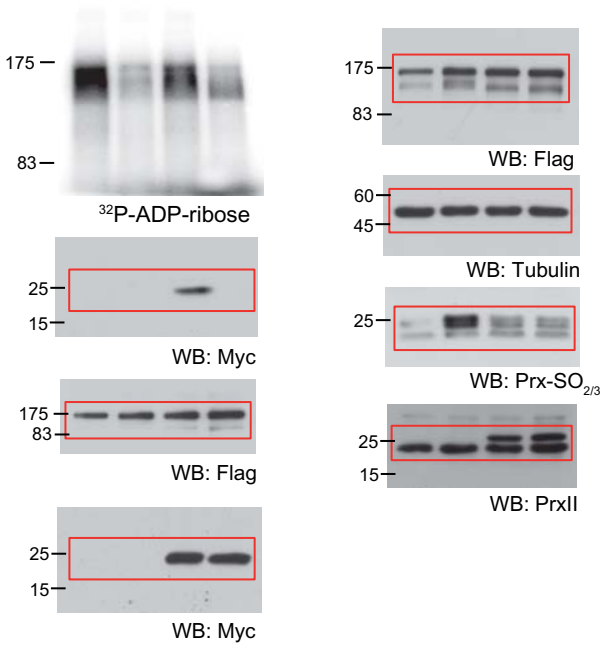

Supplementary Fig 10 Continued

Supplementary Figure 3a

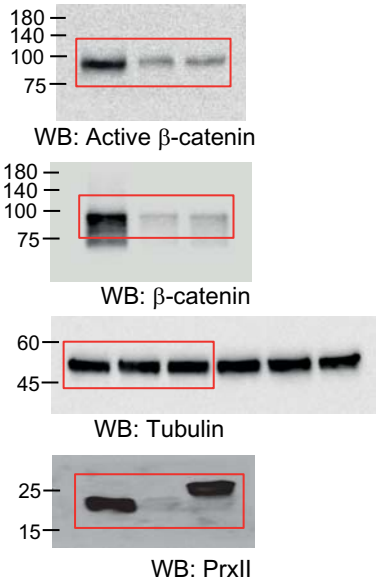

Supplementary Figure 4a

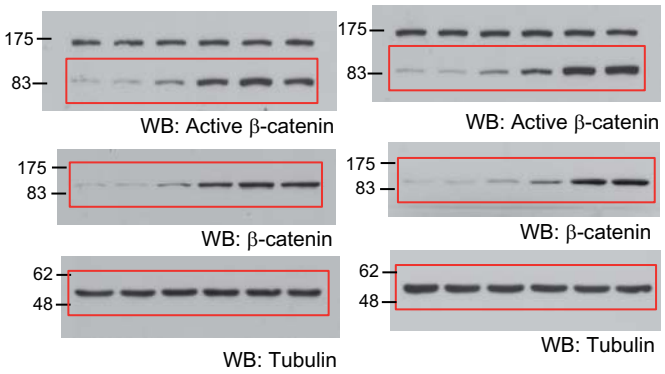

Supplementary Figure 4b

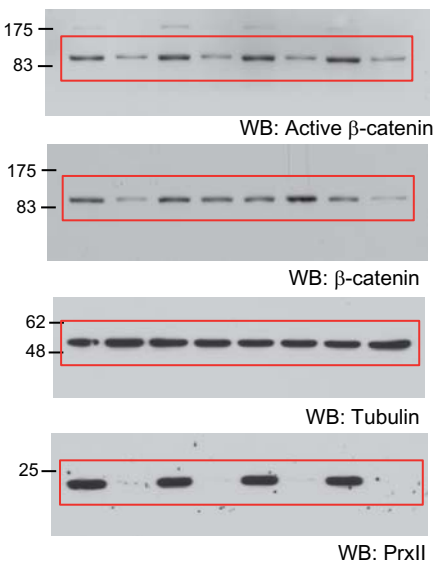

Supplementary Figure 4c

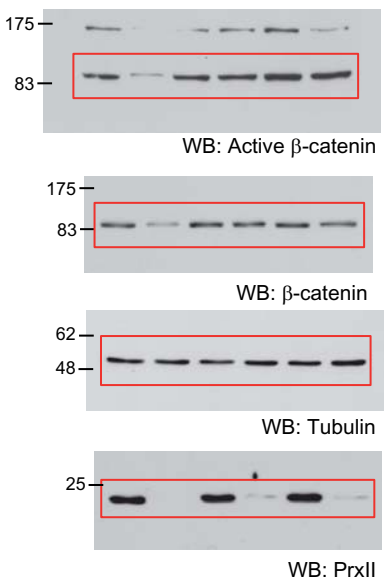

Supplementary Figure 4e

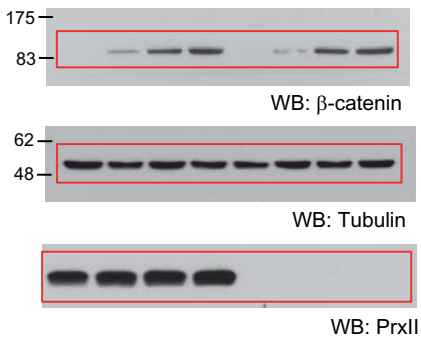

Supplementary Figure 4d

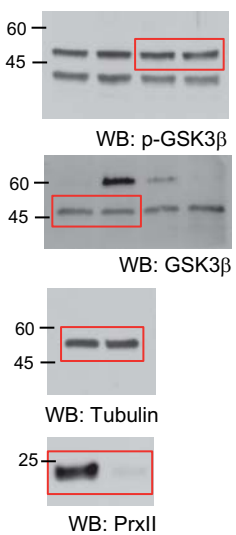

Supplementary Figure 6